Water Resources Research

RESEARCH ARTICLE
10.1029/2020WR028425

Key Points:
- Hierarchical clustering using historical data identified three classes and nine subclasses of seasonal flow regimes for Alaska
- Rainfall, snowmelt, and high-elevation melt drive a range of seasonal streamflow patterns and create mixed populations of peak streamflows
- Associations of seasonal flow regimes with elevation and climate improve understanding of hydrologic change in rapidly changing cold regions

Supporting Information:
- Supporting Information S1

Correspondence to:
J. Curran,
jcurran@usgs.gov

Citation:
Curran, J. H. & Biles, F. E. (2021). Identification of seasonal streamflow regimes and streamflow drivers for daily and peak flows in Alaska. *Water Resources Research*, *57*, e2020WR028425. https://doi.org/10.1029/2020WR028425

Received 22 JUL 2020
Accepted 8 DEC 2020

Identification of Seasonal Streamflow Regimes and Streamflow Drivers for Daily and Peak Flows in Alaska

Janet H. Curran[1] and Frances E. Biles[2]

[1]U.S. Geological Survey, Anchorage, AK, USA, [2]U.S. Department of Agriculture, Forest Service, Pacific Northwest Research Station, Juneau, AK, USA

Abstract Alaska is among northern high-latitude regions where accelerated climate change is expected to impact streamflow properties, including seasonality and primary flow drivers. Evaluating changes to streamflow, including flood characteristics, across this large and diverse environment can be improved by identifying the distribution and influence of flow drivers. Using metrics of mean monthly streamflow data from 253 streamgages, seasonal flow regimes were clustered to guide identification of seasonal flow drivers and form hydrologic groups for identification of peak-flow populations. Nine seasonally distinct subclasses described variability within three classes dominated by (mostly fall) rainfall, (spring) snowmelt, and (summer) high-elevation melt. The most glacierized basins exclusively grouped into high-elevation melt subclasses, and less glacierized basins sometimes exhibited seasonal patterns aligned with rainfall-dominated and snowmelt-dominated regimes. Peak-flow populations varied by subclass from dominant rainfall or dominant snowmelt to mixed rainfall–snowmelt or mixed rainfall, snowmelt, and high-elevation melt. Within subclasses, rainfall generated higher mean peak flows (relative to mean annual flow) than snowmelt or high-elevation melt. Seasonal flow regimes showed clear but complex associations with basin characteristics, primarily elevation and winter temperature, and with geographic location. These dependencies provided elevation-based analogies for changes associated with warming and insights for seasonal flow regime prediction and hydrologic region delineation. These results provide a spatially comprehensive perspective on seasonal streamflow drivers across Alaska from historical data and serve as an important historical basis for analysis.

1. Introduction

Northern high-latitude cold regions are one of the forefronts of 20-century and 21-century climate change (IPCC, 2014; Markon et al., 2018; Walsh et al., 2011). In Alaska, projected warming is expected to continue declines in glacier mass and increase rain-to-snow precipitation fractions, while projected precipitation patterns are expected to vary spatially (Arendt et al., 2002; Bieniek et al., 2014; Lader et al., 2017, 2020; Littell et al., 2018; Markon et al., 2018; S. A. McAfee et al., 2013; S. McAfee et al., 2014; Walsh et al., 2018; Wouters et al., 2019). How these climate trends will translate to changes in streamflow patterns, especially flooding properties, depends on the type and relative dominance of streamflow-generating processes, or drivers, in a diverse environment that includes temperate and boreal forests, Arctic tundra, and 12% of the world's glacier area (RGI Consortium, 2017; Viereck et al., 1992). Characterizing historical streamflow patterns and their underlying drivers thus creates an important basis for understanding and planning for the impacts of climate change, which has critical implications for engineering design, public safety, and ecosystems (Bunn & Arthington, 2002; Milner et al., 2009; Wilby & Keenan, 2012).

Primary streamflow drivers form distinct seasonal patterns of streamflow, or seasonal flow regimes, which can be effectively characterized by a hydrograph of long-term mean daily or mean monthly streamflow (Krasovskaia et al., 1999). Hydrograph shape, along with geographic location, climate, and basin characteristics, can be used to infer these drivers (Weingartner et al., 2013). Regional patterns of drivers across Alaska are likely complex as they depend on climate and geography that can be both varied and extreme (Eaton & Moore, 2010; Shulski & Wendler, 2007). For example, regions of flood response to climate change for the contiguous United States and northern Europe are often a patchwork (Archfield et al., 2016; Matti et al., 2017) showing a range of responses at multiple scales (Mastin et al., 2016; Slater & Villarini, 2016). Alaska has sparse, short, and often discontinuous streamflow records and is often excluded from continental-scale studies (e.g., Berghuijs et al., 2016). However, as for other cold regions (Matti et al., 2017), large-scale regional differences in climatic forcing (Bieniek et al., 2012) likely form an important control on Alaska flow regimes, moderated by basin-specific factors such as glacier coverage, elevation, and permafrost coverage.

Classification of hydrologic characteristics creates intuitive categories that can help refine understanding of regional hydrology (Matti et al., 2017; Olden et al., 2012) and disentangle complex multidriver streamflow patterns. In regions that store snow and ice, seasonal melt processes and rainfall are primary drivers often out of phase with each other. In Alaska, melt-based drivers can be partitioned by source as snowmelt or glacier melt (Beamer et al., 2016; Hill et al., 2015), which controls availability, and by elevation, which dictates timing. Chapman (1982) described seasonal streamflow patterns generated by rainfall, low-elevation snowmelt, high-elevation snowmelt and glacier melt, and glacier-dammed lake outburst floods and noted low-flow summers in coastal southeast Alaska and low winter base flows followed by break-up–freeze-up patterns over much of the rest of the state. Subsequent informal studies recognized coastal, interior, and glacial streamflow patterns statewide (Wiley & Curran, 2003) and varying combinations of glacial, snowmelt, and rainfall drivers in localized studies (Brabets et al., 1999; Curran, 2012; Edwards et al., 2013). More formalized flow regime classifications along the Gulf of Alaska using modeled (Sergeant et al., 2020) or observed data (Todd et al., 2017) collectively found classes with single or multiple rainfall, snowmelt, and glacier-melt drivers and additional classes recognizing the influence of lake storage or groundwater. Comprehensive flow regimes include fundamental elements described as magnitude, frequency, duration, timing, and rate of change of streamflow (Poff et al., 1997) captured from multiple stochastic streamflow metrics (Archfield et al., 2014). To date, no formal statewide classification of such flow regimes, or seasonal flow regimes, which address the timing aspect of the flow regime, exists.

In this study, we present hierarchical clusters of seasonal flow regimes for Alaska developed from observed streamflow data and infer the associated dominant daily streamflow drivers. Within the clusters, we also explore aggregate peak-flow seasonality to identify multiple populations of peak flows (Ryberg et al., 2016) and infer dominant peak-flow drivers. Our intent is to provide a framework of historical seasonal flow regimes and dominant drivers for Alaska from which the impact of anticipated future changes can be evaluated.

2. Study Area

The U.S. state of Alaska is a topographically complex region that encompasses 1.5M km^2 in temperate to polar environments (Figure 1(a)). Bounded by the Pacific Ocean on the south and by the seasonally ice-covered Bering Sea and Arctic Ocean on the west and north, Alaska contains extensive areas of wetlands, lakes, tundra, forests, and permafrost, interspersed with mountain ranges and glaciers. The headwaters of some streams, especially in the Yukon River basin and in southeast Alaska, extend across the eastern border into Canada. Alaska has a complex and diverse climate (Shulski & Wendler, 2007) that has been described regionally in 13 climate divisions (Bieniek et al., 2012). We simplify this to three general zones to capture primary differences: (1) a maritime South Coastal region consisting of the coastal areas bordering the Gulf of Alaska and North Pacific Ocean and including the transitional maritime-continental Bristol Bay and Cook Inlet basins; (2) a mostly continental Interior region that also includes part of the Copper River basin and the more moderate western coastal area; and (3) an Arctic region extending northward from the crest of the Brooks Range (the North Slope; Figure 1(a)).

Temperature variability and extremes vary with latitude and with distance from the ocean (Figure 1(b)). South Coastal areas experience relatively mild and less variable temperatures, whereas the seasonal presence of sea ice limits the moderating effect of the ocean on temperatures along the coast farther north. The Arctic has the lowest mean annual temperature (−12°C); however, the record low (−62°C) and high (38°C) temperatures occurred in the continental Interior (Shulski & Wendler, 2007). Temperature, precipitation, and storm tracks are also influenced by the height and distribution of prominent mountain ranges (Figure 1(a)). Alaska precipitation (Figure 1(c)) reaches extreme highs in the South Coastal region as abundant moisture transported onshore from the Pacific Ocean interacts with the mountainous terrain, drops substantially moving into the Interior, and decreases to extreme lows on the coastal plain of the Arctic region (Stewart et al., 2017). Atmospheric rivers (ARs), bands of moisture-laden air advected across the Pacific Ocean from lower latitudes, can occur any time of year, deliver heavy rain or snow to many

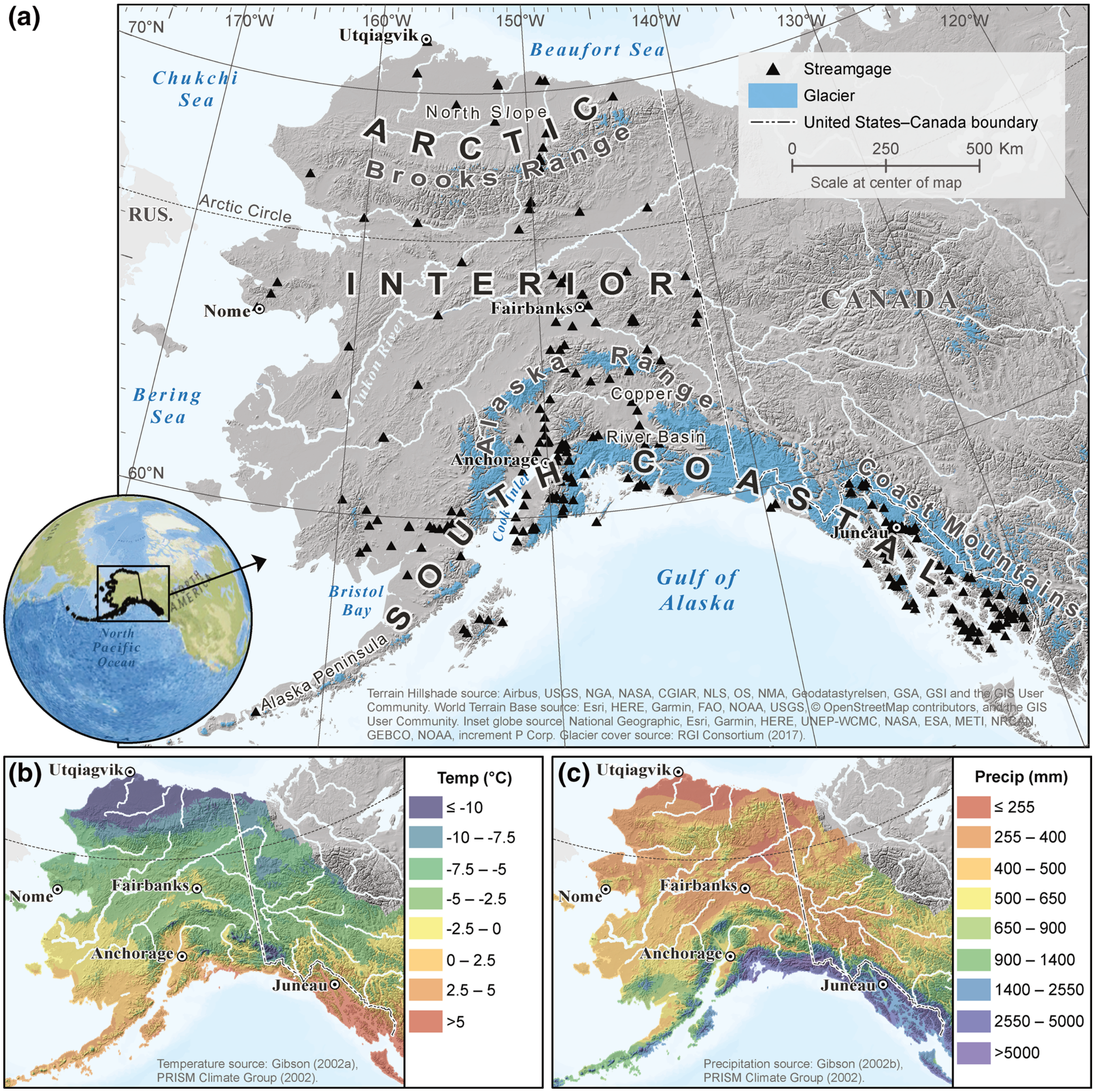

Figure 1. Characteristics of study area, including (a) physical features and location of streamgages used in the analysis (streamgages listed in Curran and Biles [2020]), (b) mean annual temperature, and (c) mean annual precipitation.

parts of the state, and cause extreme floods (Papineau & Holloway, 2011). ARs are most common in South Coastal (Guan & Waliser, 2015), where the number of events typically peaks in August–October (Mundhenk et al., 2016; Sharma & Déry, 2019). Rain-on-snow (ROS) events, in which streamflow is generated by snowmelt and rainfall, occur across Alaska, most commonly in the western Interior and South Coastal regions (Bieniek et al., 2018; Pan et al., 2018) and most frequently October–April (Bieniek et al., 2018). ARs combined with ROS events (Crawford et al., 2020; Guan et al., 2016) can lead to substantial flooding (McCabe et al., 2007). Outside South Coastal, precipitation falls mainly in summer–mid fall in the form of frontal systems and convective storms, with convective storms especially common in the Interior in June and July (Farukh et al., 2011; Papineau & Holloway, 2011; Shulski & Wendler, 2007).

The amount of snow and ice and the timing of the melt period play a significant role in Alaska streamflow regimes. Snow covers the ground in much of the state for at least half the year, and snowfall amounts vary with climate and elevation, from an annual average of 76 cm year^{-1} in the dry Arctic to the highest observed winter snowfall of 24.7 m in the South Coastal mountains (Shulski & Wendler, 2007). Glaciers and icefields occupy 4% of Alaska (63,803 km^2; RGI Consortium, 2017), of which 99% are distributed throughout the southern third of the state where precipitation is highest (Figure 1). In the Arctic, snow typically melts within a 7–10-day period between April and June (Kane et al., 2008). In contrast, snow melts over a longer period between March and May in other regions. Snowmelt is often delayed as elevation increases (Lader et al., 2020; Lundquist et al., 2004), creating a more gradual and prolonged snowmelt runoff pattern for basins that include a large elevation range. Glaciers further influence runoff seasonality through release of meltwater at various time scales (Fountain & Tangborn, 1985; Jansson et al., 2003). Snowmelt from the glacier surface is delayed and ice melt reaches a maximum in summer when temperature and sun angles are highest and albedo is reduced (Hock et al., 2005). For this study, we consider high-elevation processes to include delayed snowmelt from high elevations, additionally delayed melt from glacier snow cover and ice in glacierized basins, and (in some cases) summer precipitation, that collectively keep streamflow elevated throughout summer. Permafrost, which is continuous in the Arctic and discontinuous over much of the rest of the state, thaws to a shallow active layer that limits soil moisture storage and can intensify flooding (Kane et al., 2004). Cold-region flood-generating processes not addressed in this study include ice-jam flooding during spring break-up, which rarely produces annual peak flows, and glacier lake outburst floods, which strongly depend on local conditions.

3. Methods

The study identified classes of similar seasonal streamflow patterns to provide groups for aggregating streamflow driver information. To accommodate a sparse streamgaging network, we leveraged short streamflow records through use of metrics of daily flow, which average to a representative pattern relatively quickly. We clustered stream sites using mean monthly streamflow, calculated from daily streamflow, which has been used as a measure of timing in more comprehensive explorations of flow regimes (Olden et al., 2012). Months used for clustering were selected to minimize correlation and provide detailed differentiation of seasonal patterns. The seasonal flow regime clusters were then used to identify daily and peak-flow population drivers. Basin characteristics and weather station observations were used to support the interpretations of drivers and were explored as explanatory variables of differences in seasonal flow regimes.

3.1. Streamflow Data and Basin Characteristics

Streamgage information was compiled for an initial data set of U.S. Geological Survey (USGS) streamgages in Alaska that had at least 5 years of daily streamflow data. Mean daily streamflow typically converged to a representative hydrograph shape within 5 years, a record length consistent with other studies of seasonal streamflow patterns (Kuentz et al., 2017; Shanley & Albert, 2014). To obtain a representative spatial sample, periods of record were not limited to concurrent periods with other streamgages or to phases of the Pacific Decadal Oscillation or other teleconnections shown to affect seasonal streamflow patterns in Alaska (Fleming et al., 2016). As a result, the data set represents an inventory of historical conditions but not necessarily concurrent conditions. The Aleutian Islands, Bering Sea islands, and selected areas in interior and western Alaska lacked sufficient streamgage data to be well represented by this study.

Of the initial 331 streamgages, 253 streamgages met the following additional criteria: (1) at least 5 years of daily mean streamflow unaffected by regulation, urbanization, or outburst floods (including glacial lake outburst floods), (2) a definable drainage area no smaller than 1 km^2, and (3) not hydrologically redundant with another streamgage. Screening included consideration of USGS annual peak-streamflow file data codes and annual data reports (U.S. Geological Survey, 2019; https://wdr.water.usgs.gov/). Hydrologically redundant streamgages were defined as nested streamgage pairs having a drainage area ratio (larger divided by smaller) less than 5. Redundant pairs were reduced to the longer-record streamgage, except for the very large Yukon River, where the smallest drainage area was selected for comparability to other streams. Study data, including periods of record used and omitted and reasons for omission for streamgages not used, are presented in a separate data publication (Curran & Biles, 2020).

Hydrologic data for analyses of the selected streamgages included daily mean streamflow and annual maximum instantaneous (peak) streamflow. Streamflow data were obtained from the USGS National Water Information System (NWIS) (U.S. Geological Survey, 2019) through water year 2017, where a water year is defined as the period from October 1 to September 30 of the following year and named for the calendar year in which it ends. Daily mean streamflow data were edited to omit the following: an entire water year if ineligible conditions occurred in any part of the year, records for February 29, and partial water years (missing more than 1 day) using the conventional October–September period, except at seven sites where data were collected on a water year defined by alternate months. Daily mean streamflow was then used to compute mean daily, mean monthly, and mean annual streamflow for the period of record meeting study criteria. Peak-flow data were edited to remove peaks coded as outburst, regulated, or historic (collected outside the systematic gaging period), and peaks occurring on February 29 were assigned a date of February 28. Because peak flows were aggregated by a cluster group for analysis, no minimum record length was required; peak-flow records were shorter than 5 years for 2% of study streams. Median record lengths for data used in the analysis were 13 years for daily flows and 16 years for peak flows.

Study basin characteristics (Curran & Biles, 2020) consisted of an expansion of Appendix A of Curran et al. (2016), which compiled basin centroid location and drainage area from the basin boundary; mean basin elevation from ASTER GDEM version two elevation data (National Aeronautics and Space Administration Land Processes Distributed Archive Center, 2011); mean annual precipitation and mean minimum January temperature (used here as an indicator of winter temperature) from PRISM temperature and precipitation data for Alaska (Gibson, 2009a, 2009b) and Canada (PRISM Climate Group, 2002); and percent of basin covered by glaciers from Randolph Glacier Inventory version 2.0 glacier coverage data (RGI Consortium, 2012) for most basins. For basins not in Curran et al. (2016), we used ArcGIS software (ESRI, 2017) and methods and sources described in that study to compute these basin characteristics. Additionally, we computed mean monthly precipitation and temperature for all study basins using the Curran et al. (2016) methods and PRISM data.

3.2. Cluster Analysis

A hierarchical cluster analysis of metrics of mean monthly streamflow, using months selected to best differentiate seasonal flow patterns over the entire hydrograph, was used to develop seasonal flow regime classes and subclasses. To remove the scale dependence of basin size and annual precipitation, considered primary drivers of flow magnitude (Curran et al., 2016), mean monthly streamflow was normalized by dividing by mean annual streamflow for each streamgage, creating a series of dimensionless numbers known as Pardé coefficients (Pardé, 1933). Monthly Pardé coefficients can range from 0 (no flow that month) to 12 (all the flow for the year arrives in that month) and would all equal 1 if flow did not vary by month. To remove the effect of differences in variance of normalized flow between months, the data set of Pardé coefficients was standardized by subtracting the mean and dividing by the standard deviation across all sites, resulting in flow variables consisting of monthly Pardé z-scores.

Strongly correlated variables, which generally exceeded a Pearson's correlation coefficient (r) of about 0.8, were identified from a scatterplot of monthly Pardé coefficient pairs (Curran & Biles, 2020). A principal component analysis (PCA; computed using the correlation matrix with *princomp* in the R package *stats*) of all variables and then successive iterations of selected variables was used to generate PCA scores and biplots (Figure S1) that informed removal of variables to minimize multicollinearity. Of the strongly correlated cold season flow variables—November–March and to some degree October and April–February best represented the lowest flows of winter. May captured much of the variability in the snowmelt period. For the strongly correlated pair of July and August, July was chosen as the variable with the best performance at differentiating summer streamflow seasonality. Initial cluster analysis using these three monthly Pardé z-scores successfully differentiated seasonal streamflow patterns except for a group of Arctic streams so strongly snowmelt dominated that flows were only notably high in June. The June flow variable was included to capture this narrow seasonal window. The fall month of September was considered but explained little variation and was removed, leaving February, May, June, and July Pardé *z*-scores as the selected monthly flow variables for clustering.

Cluster analysis used Euclidean distance and Ward's minimum-variance agglomerative method (*ward.D2*) and was computed using *hclust* within the R package *stats* (R Core Team, 2018). This hierarchical clustering method results in a dendrogram of nested clusters and allows the user to choose the number of clusters. For this study, two nested groupings were useful: the smallest number of clusters that contained distinct seasonal differences (classes), and the largest number of clusters before cluster population dwindled and distinction of seasonal differences blurred (subclasses). The specific selection relied on the rate of proliferation of clusters on the dendrogram, the visual similarity of mean daily streamflow plots in proposed clusters, and silhouette plots, which show the strength of the similarity of a site to other sites in its cluster relative to sites in other clusters (Rousseeuw, 1987). Silhouette plot scores varied little between number of clusters for the class and subclass levels, requiring more interpretation using the other screening processes. For ease of visualization, subclasses were arranged within the classes in increasing order of melt dominance and identified using the class number plus a letter.

3.3. Peak-Streamflow Timing

Visualizing the timing of peak flows for a group of streams as a frequency distribution of their day of year of occurrence can help identify the most common peak-flow periods (Ryberg et al., 2016). Using this technique, a density curve of peak day of year is computed for the aggregated peak flows and a local minimum in the curve can be used to denote the date dividing two populations of peaks, each assumed to be generated by different streamflow drivers. For this study, where peaks could be attributed to more than two primary drivers, the methods of Ryberg et al. (2016) were expanded to examine all feasible local minima in the day-of-year density curve. Density curves for peaks in each subclass were prepared using *density* in R after weighting each peak by the record length of its streamgage to adjust for periods of record ranging from 2 to 98 years. We used *turnpoints* in the R *pastecs* package (Grosjean & Ibanez, 2018) for computation of locations and statistics of local minima and used those statistics and the likely range of dates of melt or rainfall seasons observed from patterns in subclass hydrographs to guide selection of local minima as the date dividing clusters of peaks where possible. For subclasses where density curves did not form a valley in an anticipated period but did form an inflection point, the inflection point was adopted. An inflection point provides less confidence than a local minimum and encourages caution when interpreting dates used as population boundaries. Inspection of hydrographs indicated that this condition was common in subclasses with summer rainfall or summer melt where the separation between populations was small or gradational.

3.4. Attribution of Streamflow Drivers

When multiple streamflow drivers are present, the hydrograph can be considered a mixture of unimodal distributions, each having its own variance (normalized flow magnitude) and mean (flow timing). Class and subclass median hydrographs were prepared from Pardé coefficients, and mean daily streamflow, normalized by mean annual flow, was used to generate a median hydrograph and the 10th–90th percentile envelope of mean daily flow for each subclass. From these composited hydrographs and variability envelope, the number, timing, and magnitude of hydrograph modes and the relative magnitude of summer flows provided readily distinguishable characteristics of the subclasses that fit patterns associated with drivers. Drivers considered included low-elevation snowmelt, high-elevation snowmelt, glacier melt (assumed to be accompanied by high-elevation snowmelt), rainfall (in various seasons), or a mixture of these processes. Preliminary inferred driver interpretations were then supported by basin and climate characteristics. Class and subclass mean basin elevations and glacier coverage helped verify the potential for high-elevation melt processes as a dominant driver. Mean monthly streamflow response to mean monthly basin temperature and precipitation for individual streamgages helped identify dominance of melt-based and rainfall drivers, respectively. Interpretation of drivers was also aided by viewing scatterplot pairs of subclass-averaged Pardé coefficients and monthly precipitation or temperature (similar to the precipitation-runoff polygons of Ali et al. [2014]). A line connecting monthly scatterplot pairs showed periods of strong and weak correlation to the respective climate variables.

Using the associations between flow seasonality and streamflow drivers determined for mean daily streamflow, primary drivers for peak-flow populations within each subclass were assumed to correspond to low-elevation snowmelt in the spring, high-elevation snowmelt or glacier melt in the summer for high-elevation basins, and rain in winter, summer, or fall, depending on the subclass. Seasons are used as relative references with spring and fall referring to the timing of bimodal crests in high daily flows or peak-flow density and summer referring to July plus parts of June or August to account for variations in timing between subclasses. ROS was considered as a separate process, but no ready means to identify groups of ROS peaks emerged because ROS events can occur over a range of seasons and overlap with other drivers.

To verify that the inference-based peak-driver determination reasonably reflected streamflow-generation mechanisms, the streamgage hydrograph closest to each subclass median was selected for comparison to weather records. For the day of, and up to 3 days preceding, the peak, daily mean streamflow patterns were compared to patterns in available daily temperature and precipitation records from U.S. (National Oceanic and Atmospheric Administration, 2019) and Canadian (R package *weathercan*, LaZerte & Albers, 2018) weather stations within the basin (Table S1). Rigorously verifying streamflow drivers for all peaks would have required characterization of basin weather and runoff-generation processes beyond the scope of this study, but weather patterns from these selected stations provided a first-order check on group assignment of peak-flow drivers.

4. Results

4.1. Seasonal Streamflow Regimes

Clustering resulted in three classes that captured primary differences in Alaska hydrograph shapes (Figure 2(a)) and had high-flow mode timing readily associated with streamflow drivers: a rainfall-dominated (Rain) spring-snowmelt/fall-rainfall regime, a snowmelt-dominated (Snow) spring-snowmelt/fall-rainfall regime, and a summer high-elevation-melt-dominated (High-elevation melt) regime. Most streams (83%) in the High-elevation melt class were glacierized. Each class split at least once to form nine subclasses that better captured the diversity of seasonal flow regimes (Figure 2(b)). Each primary class driver dominated one subclass (1A, 2D, and 3C, respectively). The remaining subclasses, and the preponderance of the individual study streams (Figure 3), consisted of hybrid seasonal flow regimes from mixed drivers. Class membership of individual streams and position on the cluster dendrogram (Figure S2) are presented in Curran and Biles (2020).

Classes varied by overall seasonality (dependence on seasons, as measured by the range of Pardé coefficients; Table 1) and by the number, timing, and relative magnitude of modes (Table 1 and Figure 4(a)). Subclasses varied primarily by timing and magnitude of spring and summer flows (Figure 2(b) and Table 1). Within-subclass variability, as indicated by the width of the 10th–90th percentile flow envelope (Figure 4(a)), was slightly less for spring-snowmelt and summer high-elevation melt periods than for summer or fall-rainfall periods across all groups. High variability apparent during winter/spring periods in cold-winter subclasses relates to variations in low-flow drivers not addressed here and to measurement errors associated with flow under ice. Statistically compiled subclass median daily hydrographs (Figure 4(a)) were similar to the streamgage hydrographs closest to the medians (Table 1); both showed representative mode and intramode magnitude and timing. Day-to-day streamflow variability, seen as high-frequency oscillations in the hydrographs, was greater during rainy periods. Seasonal flow regimes formed associations with basin characteristics, primarily elevation, climate, and geographic location (Figures 5 and 6). Drainage areas spanned at least 1 order of magnitude within subclasses and overlapped between subclasses, confirming that seasonal patterns were not strongly controlled by basin size.

Streams in the Rain class mostly occurred in the South Coastal region (Figures 1 and 6). High annual precipitation, mean minimum January temperatures not far below freezing, and mean elevations generally below 500 m (Figure 5) facilitated mild seasonality and rain-dominance. Streamflow was strongly positively correlated with precipitation almost all year for subclass 1A and in fall and winter for subclass 1B (Figure 7(a)).

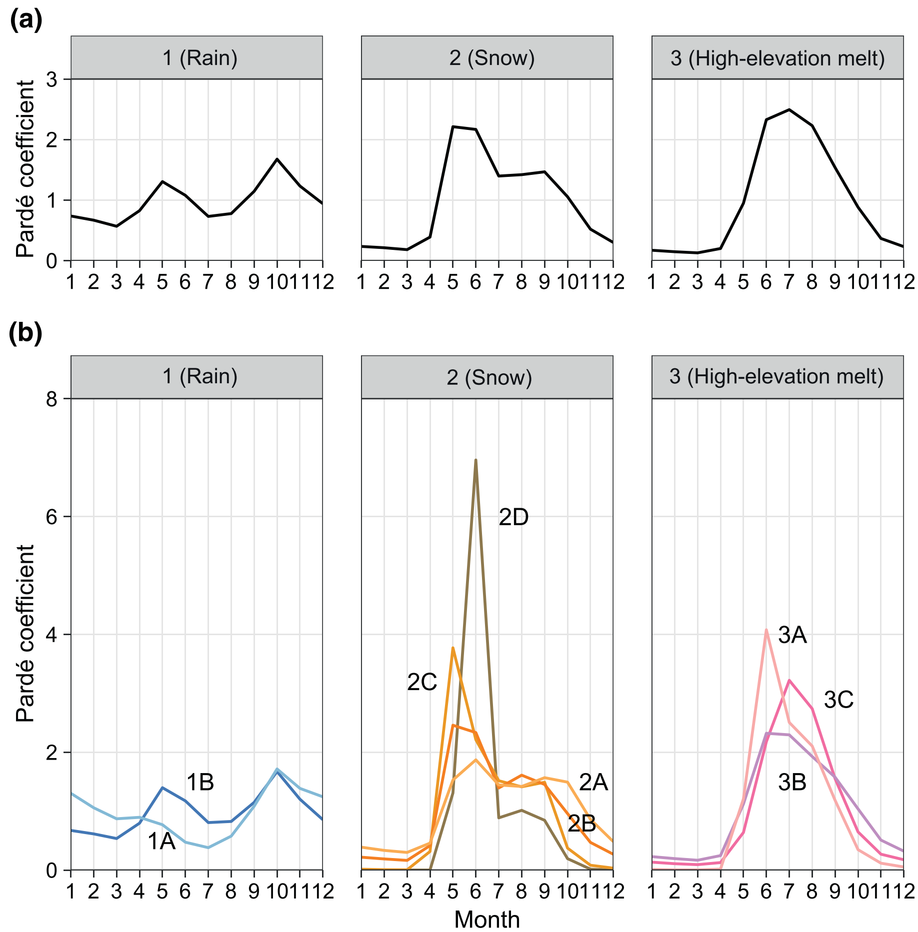

Figure 2. Group medians of mean monthly Pardé coefficients for (a) three classes and (b) nine subclasses of seasonal flow regimes for Alaska.

Snowmelt influence on daily flows increased from negligible in 1A to comparable to rainfall in 1B with increasing elevation and decreasing winter temperature (Figures 3–5).

In the Snow subclasses, snowmelt dominance increased across a latitudinal gradient of declining mean minimum January temperatures (Figures 4, 5, and 6). Streams in the mostly South Coastal, warmest-winter subclass (2A) had a mean annual basin precipitation of 2,800 mm and a snowmelt mode on average only slightly larger than the rainfall mode. In contrast, increasingly colder-winter 2B, 2C, and 2D had lower mean annual basin precipitation (dropping from 690 to 257 mm across the subclasses) and increasingly higher magnitude snowmelt modes. Subclass 2D streams, mostly located on the arctic North Slope (Figure 6), received little or no flow November–April and an average of 73% of the mean annual streamflow in May–June. For all Snow subclasses, mean monthly spring flows increased with increasing mean monthly temperature but decreased before temperatures reached a peak in July (e.g., 2B in Figures 7(b) and S3), indicating a dependence on the amount of frozen water available to melt. In selected subclass 2A basins, glaciers provided additional summer melt-based flow and generated a nearly flat-topped hydrograph where modes were difficult to discern. Although rainfall, on average, formed a secondary high-flow mode in all Snow subclasses, rainfall timing and influence varied (Table 1).

High-elevation melt class members rarely had mean basin elevations below 500 m and High-elevation melt became the exclusive class for basins with mean elevations above 1,100 m (Figure 5). The delayed and prolonged melt processes at high elevations with and without glaciers generated high midsummer (July) flows in all subclasses (Table 1 and Figure 2). The driest and coldest-winter subclass (3A) occurred in basins mostly along the Brooks Range (Figure 6), where glaciers were less common and were smaller than in less

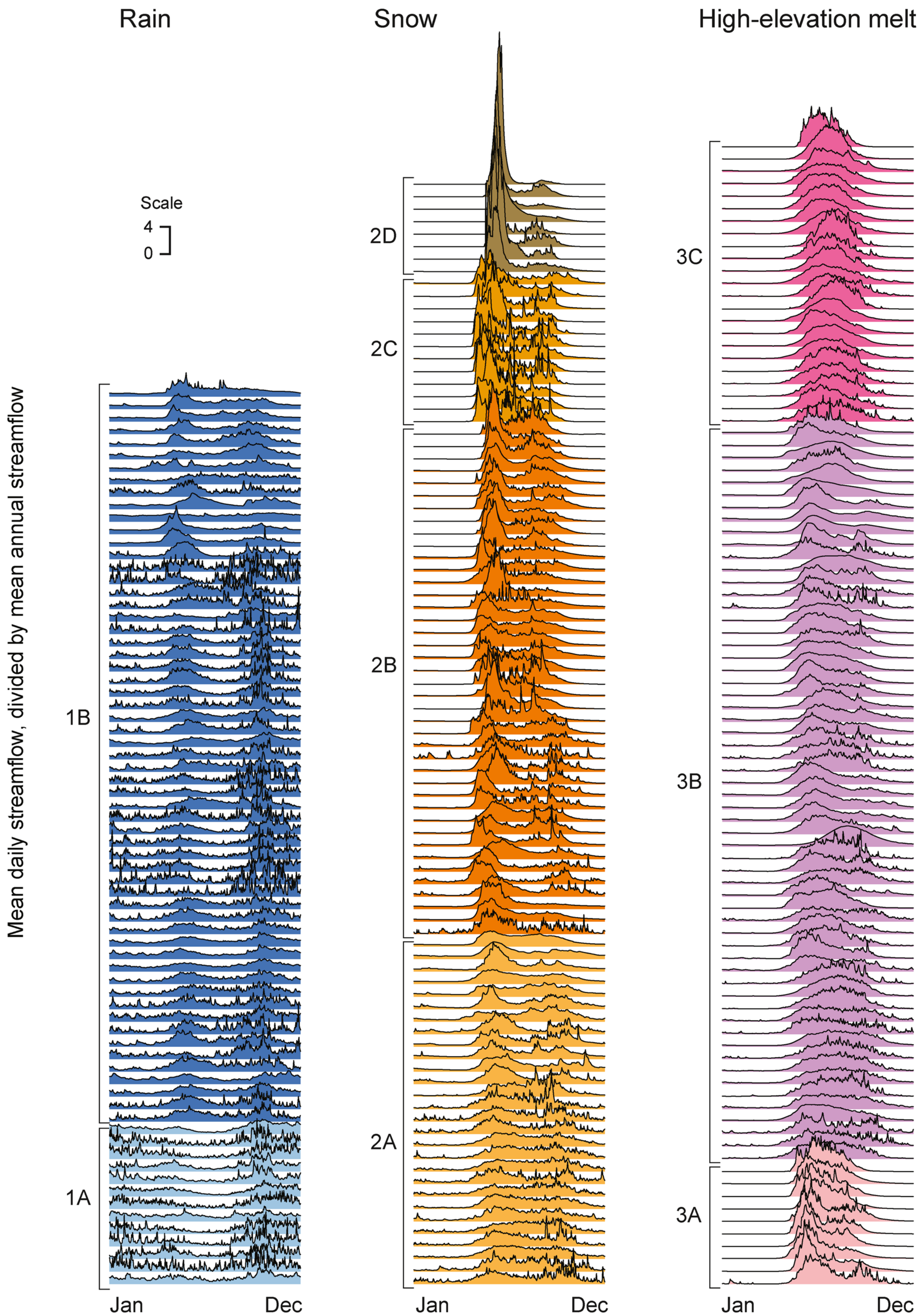

Figure 3. Hydrographs of normalized mean daily streamflow for nine Alaska seasonal flow regime subclasses, arranged by class. The *y* axis is shown on a linear scale.

10.1029/2020WR028425

Table 1

Characteristics of Streamflow Magnitude, Seasonality, and Drivers for Nine Seasonal Flow Regime Subclasses in Alaska.

Class	Distinguishing seasonal streamflow characteristics	Subclass	Representative normalized mean daily flow hydrograph[1]	Pardé coefficients: Range (min. - max.)	Pardé coefficients: Feb.	Pardé coefficients: July	High-flow mode and intramode timing, relative magnitude, and drivers	Region[2]
Rain	Mild seasonality, moderate winter flows, low summer flows. Spring snowmelt mode can be absent.	1A	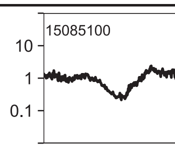	0.3-2.1	1.1	0.4	A fall-to-winter rainfall mode that peaks in October. Snowmelt can be absent or forms a mode that is smaller than the rainfall mode and peaks in April. Summer flows are the lowest flows of the year.	SC
		1B	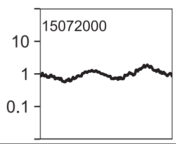	0.3-2.4	0.6	0.8	Low-amplitude, nearly equal magnitude snowmelt and rainfall modes that peak in May and October, respectively, and are separated by nearly equal magnitude summer and winter low-flow seasons. Includes streams with minimal seasonality, such as groundwater-driven streams.	SC, Int
Snow	Moderate to extreme seasonality, winter is primary low-flow season, summer is secondary low-flow season.	2A	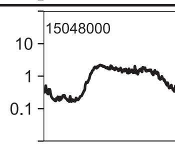	0.2-3.1	0.3	1.4	Snowmelt has a defined onset, peaks in June, and is similar in magnitude to a rainfall mode that peaks in September. The magnitude of summer flows is equal to or slightly less than spring and fall flow magnitudes.	SC, Int
		2B	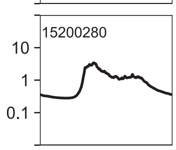	0-4.6	0.2	1.4	Snowmelt mode is well-defined, peaks in May, and is larger than a rainfall mode that peaks in September. Summer low flows are much larger than winter low flows. Rainfall timing can vary from summer to fall.	SC, Int, Arc
		2C	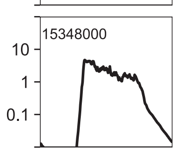	0-5.2	0	1.6	Strong snowmelt seasonality and summer rain influence. A large snowmelt mode peaks in May. Summer flows are augmented by summer rainfall and are equal to or slightly less than a subtle rainfall mode that peaks in September.	Int
		2D	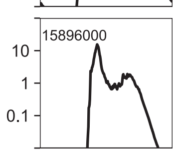	0-10.7	0	1.1	Extreme snowmelt seasonality. Most of the year's flow arrives in a short-duration and extremely large snowmelt mode that peaks in June. Rainfall produces a small and variably timed mode that peaks, on average, in August.	Int, Arc
High-elevation melt	Moderate to strong seasonality, low winter flows, high summer flows.	3A	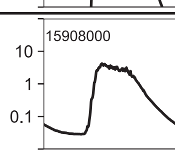	0-4.7	0	2.7	Snowmelt has a late but strong onset. Summer flows are augmented by high-elevation melt and summer rain. High-flow mode peaks in June. 40% of basins were glacierized; glacierized basins had an average of 4% glacier cover.	SC, Int, Arc
		3B	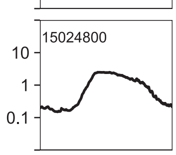	0-3.3	0.2	2.3	Moderately seasonal. Snowmelt has a dampened onset. High-elevation-melt mode peaks in July. Individual hydrographs can be symmetric about the peak or asymmetric with higher early-season flows. Rainfall can augment flows but only rarely forms a late-season high-flow mode. 83% of basins glacierized; these basins averaged 14% cover.	SC, Int
		3C	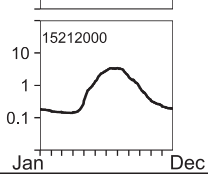	0-4.5	0.1	3.3	Strongly seasonal. Snowmelt has a dampened onset. High-elevation-melt mode peaks in July and is relatively symmetric about the peak. 100% of basins were glacierized; glacierized basins had an average of 25% glacier cover.	SC, Int, Arc

[1] USGS streamgage closest to subclass median; number indicates site ID; period of record used is presented in Curran & Biles (2020).

[2] SC, South Coastal; Int, Interior; Arc, Arctic. Regions are shown in Figure 1.

10.1029/2020WR028425

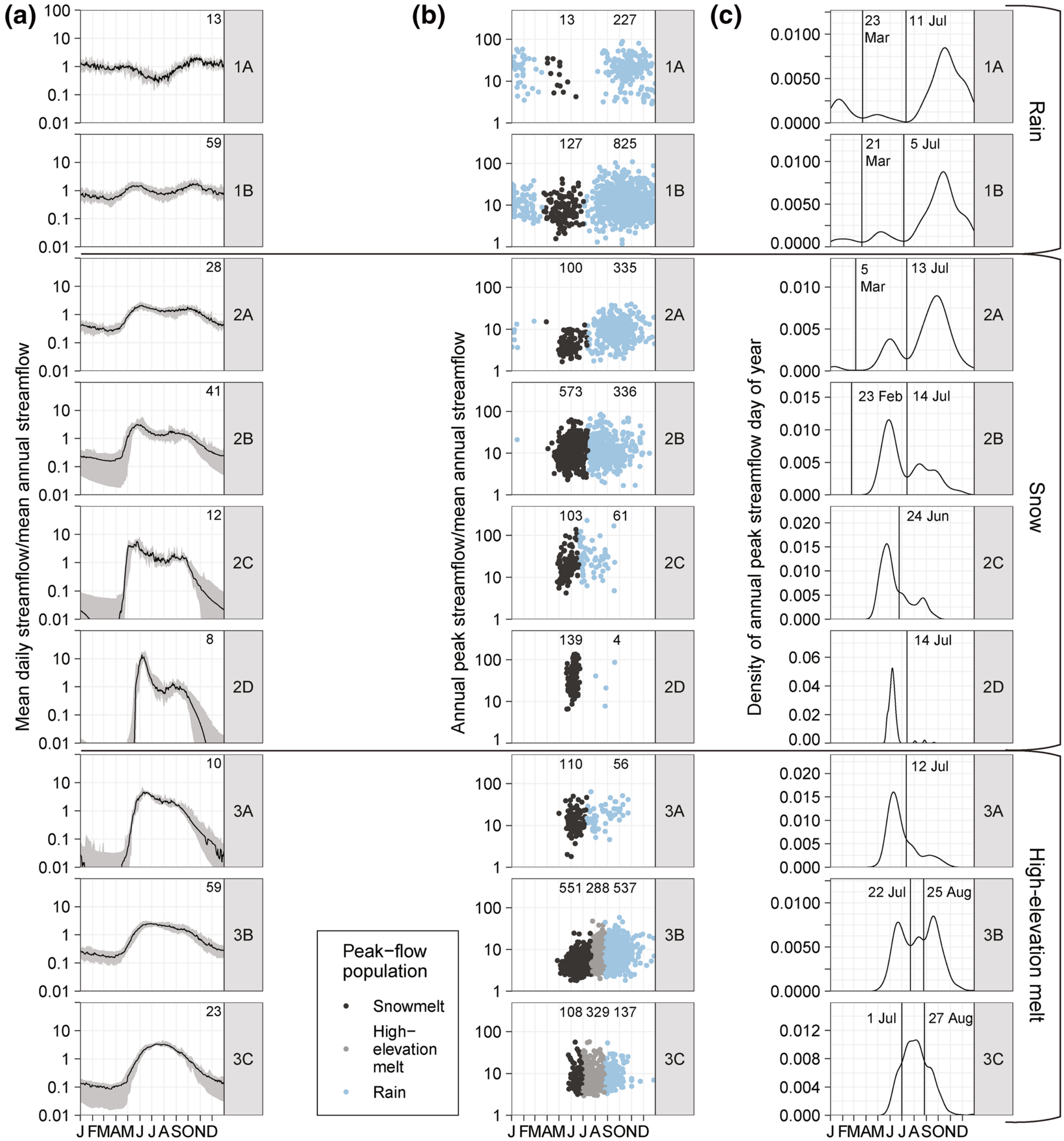

Figure 4. Diversity of seasonal patterns in mean daily and annual peak streamflow for nine seasonal flow regime subclasses in Alaska. (a) Envelope hydrographs of the 10th–90th percentile of mean daily streamflow, normalized by mean annual streamflow, and group median hydrograph (black line). Numbers indicate subclass size. (b) Annual peak streamflow, normalized by mean annual streamflow, plotted by day of year and colored by peak-streamflow population. Numbers indicate population size. (c) Density plots of annual peak-streamflow day of year. Vertical lines and dates mark the boundaries for populations in (b).

extreme climates. Subclass 3A hydrographs had a strong snowmelt pulse and were augmented by summer rain as well as high-elevation melt. In 3B and 3C, hydrographs had a more gradual snowmelt onset and variable influence of rain (Table 1). Glaciers were present in 38% of the study basins but were concentrated in subclasses 3B and 3C, which contained 75% of these and nearly all those having >8% glacier cover. The

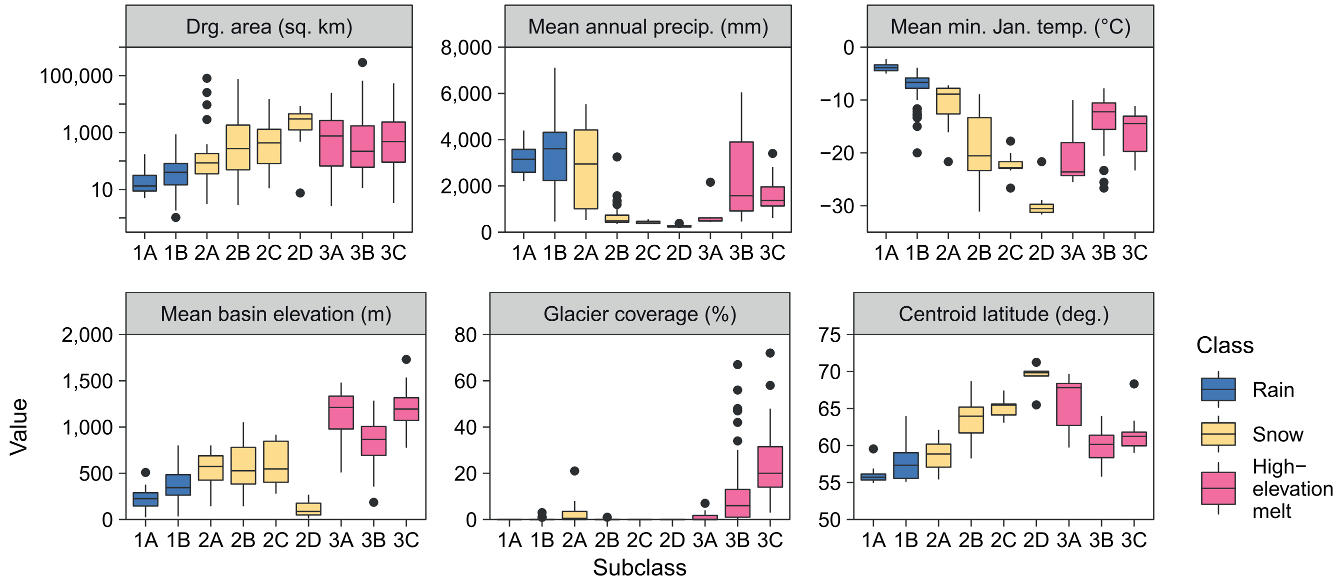

Figure 5. Values of selected basin characteristics for nine Alaska seasonal flow regime subclasses.

magnitude and relative dominance of summer flows over early-season flows (Figure 4(a)) increased with percentage of subclass glacierized and with glacier cover across 3A, 3B, and 3C (Table 1), although glacier cover varied widely in 3B and 3C (Figure 5). In the most glacial subclasses (3B and 3C), flow increased with temperature throughout summer and declined more slowly relative to temperature in fall as precipitation increased (e.g., 3B in Figure 7(b)).

4.2. Peak-Flow Populations

Aggregation of annual peak streamflows by subclass produced day-of-year density curves that showed strong to weak differentiation of 2–3 seasonal populations attributable to a dominant driver (Figures 4(b) and 4(c) and Table 2). Peaks grouped definitively into snowmelt and rainfall populations (Table 2) for subclasses having the most well-defined summer low-flow season (1A, 1B, 2A, 2B, and 2D). In the subclasses most strongly affected by summer rain (2C and 3A), peaks formed snowmelt and rainfall populations more difficult to differentiate because of the minimal gap between snowmelt and the onset of rainfall. The slight density curve inflection point used as group boundary in these subclasses likely misidentified some rainfall peaks as snowmelt peaks. In the most glacially affected subclasses, 3B and 3C, seasonal distinctions in density were also subtle (Figure 4(c)) but identified a third population, summer high-elevation melt peaks, between spring-snowmelt and fall-rainfall peaks. A local minima apparently differentiating summer and fall-rainfall peaks in 2B, 2C, and 3A was likely created by geographic differences in rainfall timing (2B and 2C; Figure 3) or the range of Interior rainfall climatologies (2C) (Farukh et al., 2011; Papineau & Holloway, 2011) and was beyond the scope of this study to resolve.

Variations between subclasses included the timing of snowmelt and rainfall-peak populations (Figure 4(c) and Table 2). The median date of spring-snowmelt peaks ranged from mid-May to mid-June, generally arriving later with colder-winter temperatures and higher mean basin elevations (Figure 5). The mix of summer, fall, and winter rain climatologies present made it difficult to generalize the factors controlling the differences in timing between subclasses. However, for the subclasses having the most discrete rainfall-peak populations (1A, 1B, and 2A), the median date of rainfall peaks varied from late September to early November, arriving later with warmer mean winter temperatures and lower mean basin elevations (Figure 5). The density of summer peaks also varied by subclass, increasing with glacier coverage from glacier-scarce 2 and 3A, where summer peaks did not form a separate population, to glacier-rich 3C, where summer peaks formed the densest population.

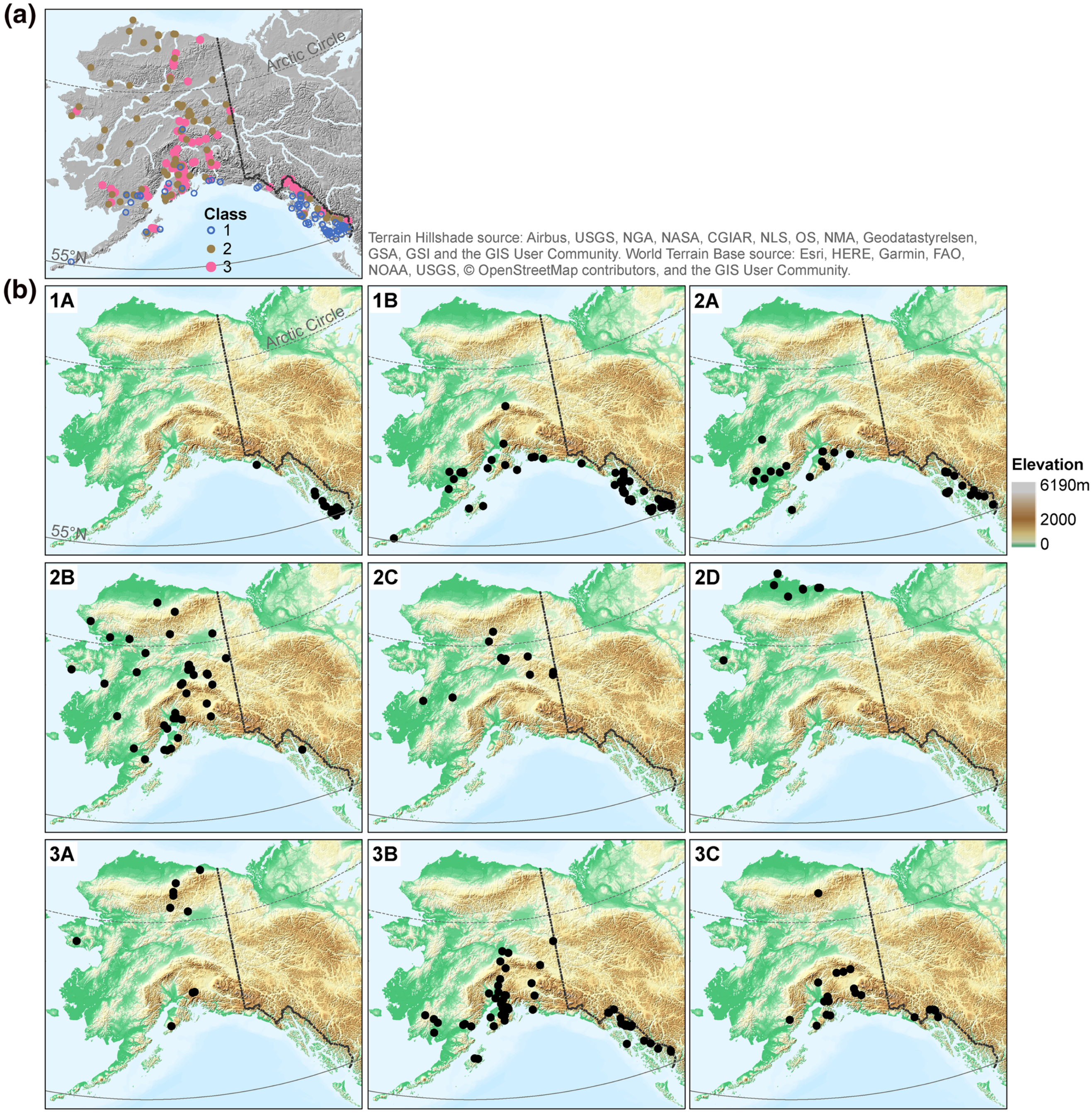

Figure 6. Geographic distribution of (a) three classes and (b) nine subclasses of seasonal flow regimes in Alaska.

The length of peak-flow seasons (Figure 4 and standard deviation in Table 2) varied by population and class. Melt-based peaks arrived in a shorter window than rainfall peaks, and Rain subclasses had the longest peak-flow seasons. Subclasses 1A, 1B, and 2A each contained a substantial winter rainfall-peak subpopulation, and subclass 1B showed a nearly year-round peak-flow seasonality (Figures 4(b) and 4(c)).

For subclasses where rainfall and snowmelt peak populations were meaningful to compare (each population >10% of total), mean rainfall peaks were consistently larger (relative to mean annual flow) than mean snowmelt peaks (Table 2). These differences were statistically significant (Mann–Whitney test on

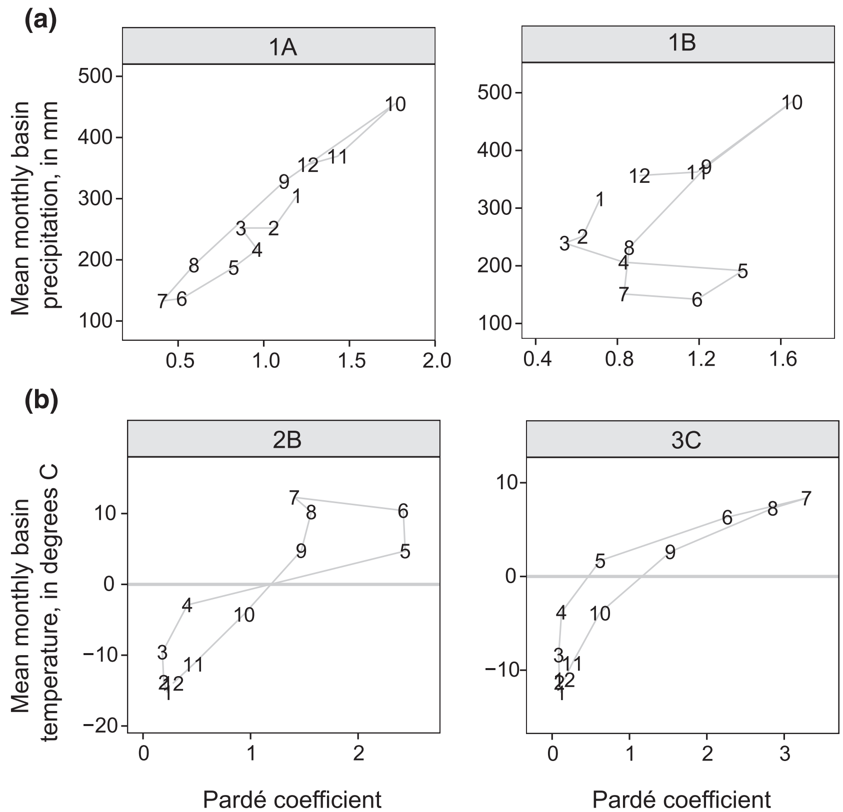

Figure 7. Examples of mean monthly streamflow–precipitation and streamflow–temperature patterns for selected seasonal flow regime subclasses: (a) Streamflow responds positively to precipitation in most months in subclass 1A and is decoupled from precipitation during the April–May snowmelt period in subclass 1B. (b) Streamflow responds positively to temperature in spring and then declines as melt sources are depleted in subclass 2B and responds positively from late spring through early winter in subclass 3C. The increase in fall Pardé coefficients over spring Pardé coefficients for the same temperature for 3C shows the additional influence of fall rainfall. Numbers correspond to months and are connected in order by the line. Plots for all subclasses are shown in Figure S3.

logs of normalized peak flow, $p < 0.05$) even though each population magnitude had a large range with considerable overlap with the other populations. For subclasses with three populations, rainfall peaks were statistically significantly larger ($p < 0.05$) than spring and summer melt-based peaks. Summer melt-based peaks were statistically significantly larger ($p < 0.05$) than spring-snowmelt peaks for 3B but nearly equal to spring-snowmelt peaks for 3C.

4.3. Streamflow Drivers

Primary peak-flow drivers (by peak-flow day-of-year density and number of peaks) matched primary daily flow drivers (by mode magnitude) for each subclass with a few exceptions (Tables 1 and 2). In subclass 2A, mean daily flows were weakly dominated by snowmelt, but rainfall peaks had a higher maximum density than snowmelt peaks and outnumbered snowmelt peaks by a factor of 3. Similarly, although snowmelt and rainfall high-flow modes in subclass 1B reached similar magnitudes, rainfall peaks outnumbered snowmelt peaks by a factor of 6. Annual hydrographs for the representative 1B streamgage showed that spring snowmelt often produced moderate to high flows for a period of days or much longer while fall rainfall produced pulses of high flows interspersed with much lower flows; both could average to similar mean daily magnitudes but fall precipitation more commonly produced the peak flow.

Table 2
Peak-Flow Population Size, Timing, and Magnitude for Nine Seasonal Flow Regime Subclasses in Alaska

		Number of peaks (% of total)			Median peak date (standard deviation in days)[a]				Mean normalized peak-flow magnitude[b]		
Class	Subclass	Snow	High-elevation melt[c]	Rain	Snow	High-elevation melt[c]	Rain	Timing of rainfall peaks	Snow	High-elevation melt[c]	Rain
Rain	1A	5		95	n/a[d]		**1 Nov. (46)**	Fall and winter	n/a[d]		18.7
	1B	13		87	11 May (23)		**17 Oct. (50)**	Fall and winter	7.4		10.9
Snow	2A	23		77	28 May (19)		**28 Sept. (35)**	Fall	4.4		8.9
	2B	63		37	**29 May (18)**		29 Aug. (34)	Summer and fall	10.4		12.0
	2C	63		37	**26 May (14)**		16 July (27)	Summer	19.8		27.2
	2D	97		3	**8 June (7)**		n/a[d]	n/a[d]	34.8		n/a[d]
High-elevation melt	3A	66		34	**10 June (13)**		24 Aug. (31)	Summer and fall	12.4		17.1
	3B	40	21	39	**20 June (17)**	10 Aug. (9)	**22 Sept. (21)**	Fall	4.5	6.6	8.0
	3C	19	57	24	18 June (8)	**30 July (15)**	16 Sept. (18)	Fall	7.2	6.8	8.7

[a]The highest-density population is shown in bold font. [b]Peak flow normalized by mean annual flow. [c]Cells are blank where no population was identified. [d]A population was identified but is too small to characterize.

Weather patterns on and near peak-flow dates for the streamgages closest to subclass medians (Table 1) logically supported inferences of primary drivers for each daily high-flow mode and peak population in most cases, and no systemic patterns appeared in misclassified peaks. However, peaks showed a dependence on antecedent streamflow conditions generated by primary or secondary drivers. Except in single-dominant-driver subclasses 1A and 2D, peaks frequently occurred as a short-term rainfall spike constructively added to relatively high antecedent daily flows driven by spring snowmelt, summer melt, or the fall rainy period. Conversely, for some low-elevation streams, peaks occurred when snowmelt contributed to a rain-dominated background flow.

5. Discussion

The seasonal flow regime classes we identified are consistent with primary flow regime categories in many studies of parts of Alaska or neighboring areas of Canada (Déry et al., 2009; Edwards et al., 2013; Sergeant et al., 2020; Wiley & Curran, 2003) except that we combine most glacial regimes with other high-elevation regimes, similar to descriptions by Chapman (1982). The subclasses served as effective bins for identifying drivers of peak-flow seasonality not confidently discernible from individual streamgage records, especially short records, although misclassifications were likely where variable rain seasonality or closely spaced seasons limited population resolution. Although not intended to capture all components of the flow regime, the classes and subclasses provide insights into variables associated with the seasonal distribution of flow, streamflow regionality, and stream sensitivity to climate change, and characteristics of the peak-flow populations help inform approaches for flood-frequency analysis.

5.1. Influences on Seasonal Flow Regimes and Peak Flows

Winter streamflow, represented by February flows in the cluster analysis, formed a first-order variable for classifying Alaska seasonal streamflow patterns, definitively separating the mildly seasonal Rain class from the strongly seasonal, melt-based classes during clustering and PCA (Figures 3 and S1). Flood seasonality was strongly influenced by winter conditions: 21% of peaks in the Rain class arrived in December–February, compared to less than 1% in the melt-based classes. Cold-winter temperatures provide an important control by facilitating storage of precipitation as snow (Lader et al., 2020) and limiting winter streamflow generation. These low antecedent streamflow conditions can provide a buffer against the flood potential of any temporary melt or rainfall-driven streamflow increases and can explain why even extreme rainfall might not generate flooding if arriving during a period of relatively low flows (Papineau & Holloway, 2011).

Summer streamflow was a defining characteristic for many subclasses (Table 1), forming annual lows in subclass 1A, annual highs in High-elevation melt subclasses, and a secondary low for most other subclasses. Varied and complex factors, including the timing of rainfall, availability and amount of meltwater runoff, evapotranspiration, and soil moisture, can affect summer streamflow.

The presence of mountainous areas, generally well represented by mean basin elevation, strongly influenced hydrograph shape and peak-streamflow drivers via generally elevation-dependent melt delay (Lundquist et al., 2004) and orographically induced rainfall. Mean basin elevation was better at differentiating subclasses than amount of glacier cover. Not surprisingly, however, the most strongly glacierized basins produced the most summer-dominated daily flows and an identifiable population of summer peaks. Orographically induced rainfall influenced summer or fall flows, depending on rainfall seasonality. This was demonstrated in streams above the Arctic Circle, which classified into three increasingly rainfall-influenced subclasses as the amount of basin headwaters located in the Brooks Range increased. Basins on the coastal plain (2D) were dominated by a short season of snowmelt-driven daily flows and peak flows. In basins mostly within the Brooks Range (3A), summer rainfall contributed to higher summer flows and more rainfall peaks than on the coastal plain, consistent with the findings of Kane et al. (2008). Arctic streams draining a partly mountainous/partly plain basin on either side of the Brooks Range (2B) showed a hydrograph influenced by rainfall less than for the mountainous streams and more than for the coastal streams.

5.2. Geographic Distribution of Seasonal Flow Regimes

Seasonal flow regime distribution revealed spatial coherence that implied a degree of geographic regionality, complicated by spatial overlap that limited simple regional definition. Spatial footprints for each subclass ranged from narrow (1A, 2D) to widespread (2B) (Figure 6(b) and centroid latitude in Figure 5). However, no major geographic or climate region (South Coastal, Interior, or Arctic) hosted only one seasonal flow regime, even at the class level (Figure 6(a)). The southeast Alaska panhandle, for example, contained at least one stream in six of the nine subclasses. Comparison to detailed Alaska climate divisions (Bieniek et al., 2012) also produced no widespread associations. The strong influence of mean basin elevation on seasonal flow regimes suggests that coupling elevation with geographic location could improve partitioning of streams into hydrologically relevant regions. For example, the distribution of subclasses identifies two primary hydrologic regions at lower elevations, a largely fall-rainfall-dominated South Coastal region (subclasses 1A, 1B, and 2A) and a spring-snowmelt-dominated Interior-and-Arctic region (2B–2D), and a summer high-elevation-melt-dominated region (3A–3C) at higher elevations across the state. Refining regional boundaries would need to consider other elements of the flow regime (Poff et al., 1997) and might be facilitated by modeling efforts that apply flow regime classifications to the landscape (e.g., Sergeant et al., 2020).

5.3. Implications for Stream Sensitivity to Climate Change

Evidence for climate-change-related streamflow shifts is widespread across northern cold regions, including changes in seasonal mean daily flow magnitude (Matti et al., 2017) and shifts in flood seasonality (Déry et al., 2009; Matti et al., 2017; Ryberg et al., 2016; Valentin et al., 2018; Vormoor et al., 2016) that differ by flow regime. The subclasses we identified can be considered nodes along a complex continuum of streamflow response to mixed flow drivers. We assume from the narrow range of either winter temperatures or precipitation for each subclass (Figure 5) that seasonal streamflow patterns isolated climate patterns to some degree. As climate changes, changing streamflow drivers can produce shifts within or along that continuum to a new node, as suggested by the identification of transitional flow regimes in Gulf of Alaska basins (Sergeant et al., 2020). For this study, overlap between subclasses depicted on PCA plots (e.g., Figure S1) and weak subclass fidelity of some streams during exploratory analysis also suggests that some streams are near a subclass boundary. The immediate likelihood of a shift is lower where environmental extremes provide buffers that can prolong driver dominance, such as for snowmelt-dominated streams on the North Slope (2D) or strongly glacierized basins (3C). The lowest-elevation streams within strongly hybrid subclasses (e.g., 1B, 2A, 2B, and 3B) thus might be among the most vulnerable to regime change given the warming of more than 2°C in the hottest temperatures and more than 5°C in the coldest temperatures expected in Alaska by midcentury relative to 1981–2000 (Markon et al., 2018).

Associations of clusters with basin elevation, winter temperature, and precipitation provide useful comparisons for understanding likely regime progressions under climate change. Using decreasing elevation as a proxy for warming supports expected progressions from high-elevation melt dominated to snowmelt dominated, and from snowmelt dominated to rainfall-dominated (e.g., Littell et al., 2018), as climate warms (Figure 5). For a visualization of a possible regime progression, consider glacierized basins across an elevation and January mean minimum temperature gradient in 3C, 3B, and 2A. The warm hydrological season (the period outside the cold-induced low-flow period) lengthens, and maximum daily flows arrive earlier, on average, across this gradient (Figure 4(a) and Table 1), in general agreement with expected changes in glacier runoff (Huss & Hock, 2018). Summer streamflow decreases and winter streamflow increases. In some subarctic systems, winter base-flow increases may result from increased glacier melt that enhances aquifer recharge (Liljedahl et al., 2017). The most common season for peak flows shifts across the warming gradient from summer to spring and fall, and the peak-flow season lengthens (Figures 4(b) and 4(c)). Similarly, a progression from snowmelt to rainfall dominated in the high-precipitation environments of South Coastal Alaska can be visualized between 2A and 1B and between 1B and 1A. In the warmer subclass of each pair, spring and summer flows are lower, winter flows are higher, and peak flows are less frequent in spring and more frequent in winter, similar to some of the climate-induced flow regime shifts observed in Scandinavia (Matti et al., 2017; Vormoor et al., 2015). These examples can provide support for modeling projected flow regimes shifts (e.g., Beamer et al., 2017; Crumley et al., 2019; Valentin et al., 2018), both in terms of verification of modeled historical conditions and comparisons of modeled future conditions.

5.4. Implications for Flood-Frequency Analysis

Mixed peak populations for a single stream can complicate flood-frequency analysis, which assumes peaks are random and homogenous (England et al., 2019). A mixed-population condition arises from differing frequency distributions of peak populations and can in many cases be addressed by analysis that separates peaks by process (England et al., 2019). The seasonal classification of peaks described here helps identify regimes in which mixed populations might have an impact on flood-frequency analysis. For example, the largest difference in mean normalized peak magnitude between snowmelt and rainfall populations occurred in subclass 2A, where snowmelt peaks were less numerous and considerably smaller. In this case, existing techniques for managing potentially influential low outliers might resolve the mixed-population differences. In contrast, most peaks in subclass 2C are snowmelt driven but rainfall peaks are larger, on average, and might warrant consideration of mixed-population analysis. Further analysis of rainfall peaks would be needed to show the degree to which rainfall-peak populations for some regimes are influenced by extreme precipitation events driven by ARs, as for the western United States (Barth et al., 2017).

5.5. Limitations

Possible biases in the data set include underrepresentation of regimes not well represented by gaging, found to include very small basins (<10 km^2) and high-elevation basins in a study for the conterminous United States (DeWeber et al., 2014). We expect that the study data set represented at least the primary streamflow drivers for these regimes. However, the lack of a groundwater-dominated or wetland streamflow class, despite several hydrographs with low-variability low-flow regimes and one relatively seasonless hydrograph (Figure 3, subclass 1B), conflicts with identification of a wetland class using modeled data for Gulf of Alaska basins (Sergeant et al., 2020). We do not expect groundwater to form a high-flow or peak-flow driver, but groundwater could be considered a driver of low flows and was not well characterized by this study. Also, although one outlet stream of a large lake showed a strongly delayed and attenuated hydrograph likely associated with temporary storage (Figure 3, subclass 3B), we could not detect a consistent pattern for lake outlets across the study data set.

Other limitations of identifying flow regimes from gaged streams include misclassification arising from local variations in streamflow. Hard clustering, unlike soft or fuzzy clustering, cannot identify strength of membership, which can make it more difficult to identify potentially misclassified or transitional members. Considering the data set and these misclassification limitations, we expect that the cluster results are suitable for identifying the primary diversity of seasonal streamflow patterns across Alaska and less reliable for identifying individual stream membership.

6. Conclusions

Clustering historical mean monthly streamflow patterns from 253 streamgages produced a systematic statewide characterization of seasonal flow regimes across the wide range of Alaska geography and climate. We identified nine seasonally distinct subclasses that nest into three classes dominated by rainfall, snowmelt, and high-elevation snowmelt or icemelt, respectively. These subclasses helped isolate the range of influence of snowmelt and glaciers in the mostly mixed seasonal flow regimes of Alaska, indicating that assessing changes to snow accumulation and melt timing and changes to glacier cover are an important aspect of understanding streamflow change in response to climate change. Snowmelt dominated high-flow modes and peak-flow populations in many streams, but in South Coastal Alaska, snowmelt had minimal influence on peak flows in low-elevation streams and larger influence on high-flow modes than peak-flow populations in many moderate-elevation streams. Glacierized basins outside the summer high-elevation-melt-dominated class have, on average, less glacier cover, milder annual seasonality, and less prominent summer high flows than glacierized basins in the high-elevation melt subclasses. Streamflow seasonality showed clear but complex dependencies on basin characteristics, especially winter temperature and elevation, which respectively suggest potential seasonal flow regime progressions with warming temperatures and a variable important for examining hydrologic regionality. The range of seasonalities and the mixes of streamflow drivers identified here indicates the utility of categorizing similar streamflow patterns as a basis for developing effective analysis of seasonal or peak flows. The characterization of streamflow drivers helps focus expectations for hydrologic change associated with climate change and identify regional hydrologic variability.

Data Availability Statement

Streamflow data used for this study are available from NWIS at https://nwis.waterdata.usgs.gov/ak/ nwis/sw, and additional supporting data are available in a USGS data release (Curran & Biles, 2020).

Acknowledgments
We gratefully acknowledge insightful comments and suggestions from C.J. Sergeant and three anonymous reviewers. Funding was provided by the Alaska Department of Transportation and Public Facilities and the U.S. Geological Survey Cooperative Water Program. We thank the many hydrologists, climatologists, and other scientists who strengthened the concepts in this paper through discussions at Alaska hydrology workshops and conferences. Any use of trade, firm, or product names is for descriptive purposes only and does not imply endorsement by the U.S. Government.

References

Ali, G., Tetzlaff, D., Kruitbos, L., Soulsby, C., Carey, S., McDonnell, J., et al. (2014). Analysis of hydrological seasonality across northern catchments using monthly precipitation–runoff polygon metrics. *Hydrological Sciences Journal*, *59*(1), 56–72. https://doi.org/10.1080/02626667.2013.822639

Archfield, S. A., Hirsch, R. M., Viglione, A., & Blöschl, G. (2016). Fragmented patterns of flood change across the United States. *Geophysical Research Letters*, *43*, 10232–10230. https://doi.org/10.1002/2016GL070590

Archfield, S. A., Kennen, J. G., Carlisle, D. M., & Wolock, D. M. (2014). An objective and parsimonious approach for classifying natural flow regimes at a continental scale. *River Research and Applications*, *30*, 1166–1183. https://doi.org/10.1002/rra.2710

Arendt, A. A., Echelmeyer, K. A., Harrison, W. D., Lingle, C. S., & Valentine, V. B. (2002). Rapid wastage of Alaska glaciers and their contribution to rising sea level. *Science*, *297*(5580), 382–386. https://doi.org/10.1126/science.1072497

Barth, N. A., Villarini, G., Nayak, M. A., & White, K. (2017). Mixed populations and annual flood frequency estimates in the western United States: The role of atmospheric rivers. *Water Resources Research*, *53*, 257–269. https://doi.org/10.1002/2016WR019064

Beamer, J. P., Hill, D. F., Arendt, A., & Liston, G. E. (2016). High-resolution modeling of coastal freshwater discharge and glacier mass balance in the Gulf of Alaska watershed. *Water Resources Research*, *52*, 3888–3909. https://doi.org/10.1002/2015WR018457

Beamer, J. P., Hill, D. F., McGrath, D., Arendt, A., & Kienholz, C. (2017). Hydrologic impacts of changes in climate and glacier extent in the Gulf of Alaska watershed. *Water Resources Research*, *53*, 7502–7520. https://doi.org/10.1002/2016WR020033

Berghuijs, W. R., Woods, R. A., Hutton, C. J., & Sivapalan, M. (2016). Dominant flood generating mechanisms across the United States. *Geophysical Research Letters*, *43*, 4382–4390. https://doi.org/10.1002/2016GL068070

Bieniek, P. A., Bhatt, U. S., Thoman, R. L., Angeloff, H., Partain, J., Papineau, J., et al. (2012). Climate divisions for Alaska based on objective methods. *Journal of Applied Meteorology and Climatology*, *51*(7), 1276–1289. https://doi.org/10.1175/JAMC-D-11-0168.1

Bieniek, P. A., Bhatt, U. S., Walsh, J. E., Lader, R., Griffith, B., Roach, J. K., & Thoman, R. L. (2018). Assessment of Alaska rain-on-snow events using dynamical downscaling. *Journal of Applied Meteorology and Climatology*, *57*(8), 1847–1863. https://doi.org/10.1175/JAMC-D-17-0276.1

Bieniek, P. A., Thoman, R. L., Walsh, J. E., & Bhatt, U. S. (2014). Using climate divisions to analyze variations and trends in Alaska temperature and precipitation. *Journal of Climate*, *27*, 2800–2818. https://doi.org/10.1175/JCLI-D-13-00342.1

Brabets, T. P., Nelson, G. L., Dorava, J. M., & Milner, A. M. (1999). Water-quality assessment of the Cook Inlet basin, Alaska—Environmental setting (Water-Resources Investigations Report 99–4025). Anchorage, AK: U.S. Geological Survey. https://doi.org/10.3133/wri994025

Bunn, S. E., & Arthington, A. H. (2002). Basic principles and ecological consequences of altered flow regimes for aquatic biodiversity. *Environmental Management*, *30*, 492–507. https://doi.org/10.1007/s00267-002-2737-0

Chapman, D. L. (1982). Daily flow statistics of Alaskan streams (NOAA Technical Memorandum NWS AR-35). Anchorage, AK: National Weather Service. ftp://ftp.library.noaa.gov/noaa_documents.lib/NWS/TM_NWS_AR/TM_NWS_AR_35.pdf

Crawford, A. D., Alley, K. E., Cooke, A. M., & Serreze, M. C. (2020). Synoptic climatology of rain-on-snow events in Alaska. *Monthly Weather Review*, *148*, 1275–1295. https://doi.org/10.1175/MWR-D-19-0311.1

Crumley, R. L., Hill, D. F., Beamer, J. P., & Holzenthal, E. R. (2019). Seasonal components of freshwater runoff in Glacier Bay, Alaska: Diverse spatial patterns and temporal change. *The Cryosphere*, *13*, 1597–1619. https://doi.org/10.5194/tc-13-1597-2019

Curran, J. H. (2012). Streamflow record extension for selected streams in the Susitna River Basin, Alaska (Scientific Investigations Report 2012–5210). Reston, VA: U.S. Geological Survey. https://pubs.usgs.gov/sir/2012/5210/

Curran, J. H., Barth, N. A., Veilleux, A. G., & Ourso, R. T. (2016). Estimating flood magnitude and frequency at gaged and ungaged sites on streams in Alaska and conterminous basins in Canada, based on data through water year 2012 (Scientific Investigations Report 2016–5024). Reston, VA: U.S. Geological Survey. https://doi.org/10.3133/sir20165024

Curran, J. H., & Biles, F. E. (2020). *Streamgage attributes, basin characteristics, and seasonal flow regimes, selected streamgages in Alaska, 1914–2017 (Data Release)*. Reston, VA: U.S. Geological Survey. https://doi.org/10.5066/P90K2Y4R

Déry, S. J., Stahl, K., Moore, R. D., Whitfield, P. H., Menounos, B., & Burford, J. E. (2009). Detection of runoff timing changes in pluvial, nival, and glacial rivers of western Canada. *Water Resources Research*, *45*, W04426. https://doi.org/10.1029/2008WR006975

DeWeber, J. T., Tsang, Y.-P., Krueger, D. M., Whittier, J. B., Wagner, T., Infante, D. M., & Whelan, G. (2014). Importance of understanding landscape biases in USGS gage locations: Implications and solutions for managers. *Fisheries*, *39*, 155–163. https://doi.org/10.1080/03632415.2014.891503

Eaton, B., & Moore, R. D. (2010). Regional hydrology. In R. G. Pike, T. E. Redding, R. D. Moore, R. D. Winkler, & K. D. Bladon (Eds.), *Compendium of forest hydrology and geomorphology in British Columbia* (Land Management Handbook 66, pp. 85–110). Victoria, BC: Ministry of Forests and Range, Forest Science Program and Kamloops, BC: FORREX Forum for Research and Extension in Natural Resources. http://www.for.gov.bc.ca/hfd/pubs/docs/Lmh/Lmh66.htm

Edwards, R. T., D'Amore, D. V., Norberg, E., & Biles, F. (2013). Riparian ecology, climate change, and management in North Pacific coastal rainforests. In G. H. Orians, & J. W. Schoen (Eds.), *North Pacific temperate rainforests: Ecology and conservation* (pp. 43–72). Seattle, WA: University of Washington Press.

England, J. F., Jr., Cohn, T. A., Faber, B. A., Stedinger, J. R., Thomas, W. O., Jr., & Veilleux, A. G. (2019). *Guidelines for determining flood flow frequency—Bulletin 17C (ver. 1.1)* (Techniques and Methods 4-B5). Reston, VA: U.S. Geological Survey. https://doi.org/10.3133/tm4B5

ESRI. (2017). ArcGIS Desktop: Release 105.1. Redlands, CA: Environmental Systems Research Institute.

Farukh, M. A., Hayasaka, H., & Kimura, K. (2011). Characterization of lightning occurrence in Alaska using various weather indices for lightning forecasting. *Journal of Disaster Research*, *6*(3), 343–355. https://doi.org/10.20965/jdr.2011.p0343

Fleming, S. W., Hood, E., Dahlke, H. E., & O'Neel, S. (2016). Seasonal flows of international British Columbia-Alaska rivers: The nonlinear influence of ocean–atmosphere circulation patterns. *Advances in Water Resources*, *87*, 42–55. https://doi.org/10.1016/j.advwatres.2015.10.007

Fountain, A. G., & Tangborn, W. V. (1985). The effect of glaciers on streamflow variations. *Water Resources Research*, *21*(4), 579–586. https://doi.org/10.1029/WR021i004p00579

Gibson, W. (2009a). *Mean precipitation for Alaska 1971–2000* (Geospatial Dataset-2170508). Anchorage, AK: National Park Service, Alaska Regional Office. https://irma.nps.gov/DataStore/Reference/Profile/2170508

Gibson, W. (2009b). *Mean average temperature for Alaska 1971–2000* (Geospatial Dataset-2170516).Anchorage, AK: National Park Service, Alaska Regional Office. https://irma.nps.gov/DataStore/Reference/Profile/2170516

Grosjean, P., & Ibanez, F. (2018). *pastecs: Package for analysis of space–time ecological series R package version 1.3.21*. Retrieved from https://CRAN.R-project.org/package=pastecs

Guan, B., & Waliser, D. E. (2015). Detection of atmospheric rivers: Evaluation and application of an algorithm for global studies. *Journal of Geophysical Research: Atmospheres*, *120*, 12514–12535. https://doi.org/10.1002/2015JD024257

Guan, B., Waliser, D. E., Ralph, F. M., Fetzer, E. J., & Neiman, P. J. (2016). Hydrometeorological characteristics of rain-on-snow events associated with atmospheric rivers. *Geophysical Research Letters*, *43*, 2964–2973. https://doi.org/10.1002/2016GL067978

Hill, D. F., Bruhis, N., Calos, S. E., Arendt, A., & Beamer, J. (2015). Spatial and temporal variability of freshwater discharge into the Gulf of Alaska. *Journal of Geophysical Research: Oceans*, *120*, 634–646. https://doi.org/10.1002/2014JC010395

Hock, R., Jansson, P., & Braun, L. N. (2005). Modelling the response of mountain glacier discharge to climate warming. In U. M. Huber, H. K. M. Bugmann, & M. A. Reasoner (Eds.), Global change and mountain regions, advances in global change research (23, pp. 243–252). Dordrecht, the Netherlands: Springer. https://doi.org/10.1007/1-4020-3508-X_25

Huss, M., & Hock, R. (2018). Global-scale hydrological response to future glacier mass loss. *Nature Climate Change*, *8*, 135–140. https://doi.org/10.1038/s41558-017-0049-x

IPCC. (2014). In Core Writing Team, R. K. Pachauri, & L. A. Meyer (Eds.), *Climate change 2014: Synthesis report. Contribution of Working Groups I, II and III to the fifth assessment report of the Intergovernmental Panel on Climate Change*. Geneva, Switzerland: IPCC. https://www.ipcc.ch/site/assets/uploads/2018/05/SYR_AR5_FINAL_full_wcover.pdf

Jansson, P., Hock, R., & Schneider, T. (2003). The concept of glacier storage: A review. *Journal of Hydrology*, *282*(1–4), 116–129. https://doi.org/10.1016/S0022-1694(03)00258-0

Kane, D. L., Gieck, R. E., Kitover, D. C., Hinzman, L. D., McNamara, J. P., & Yang, D. (2004). Hydrological cycle on the North Slope of Alaska. In Proceedings, Northern Research Basins Water Balance (IAHS Publ. 290, pp. 224–236). Victoria, Canada: International Association of Hydrological Sciences. https://doi.org/10.1017/CBO9781107415324.004

Kane, D. L., Hinzman, L. D., Gieck, R. E., McNamara, J. P., Youcha, E. K., & Oatley, J. A. (2008). Contrasting extreme runoff events in areas of continuous permafrost, Arctic Alaska. *Hydrology Research*, *39*(4), 287–298. https://doi.org/10.2166/nh.2008.005

Krasovskaia, I., Gottschalk, L., & Kundzewicz, Z. W. (1999). Dimensionality of Scandinavian river flow regimes. *Hydrological Sciences Journal*, *44*(5), 705–723. https://doi.org/10.1080/02626669909492269

Kuentz, A., Arheimer, B., Hundecha, Y., & Wagener, T. (2017). Understanding hydrologic variability across Europe through catchment classification. *Hydrology and Earth System Sciences*, *21*, 2863–2879. https://doi.org/10.5194/hess-21-2863-2017

Lader, R., Walsh, J. E., Bhatt, U. S., & Bieniek, P. A. (2017). Projections of twenty-first-century climate extremes for Alaska via dynamical downscaling and quantile mapping. *Journal of Applied Meteorology and Climatology*, *56*(9), 2393–2409. https://doi.org/10.1175/JAMC-D-16-0415.1

Lader, R., Walsh, J. E., Bhatt, U. S., & Bieniek, P. A. (2020). Anticipated changes to the snow season in Alaska: Elevation dependency, timing and extremes. *International Journal of Climatology*, *40*, 169–187. https://doi.org/10.1002/joc.6201

LaZerte, S. E., & Albers, S. (2018). weathercan: Download and format weather data from Environment and Climate Change Canada. *The Journal of Open Source Software*, *3*(22), 571. https://doi.org/10.21105/joss.00571

Liljedahl, A. K., Gädeke, A., O'Neel, S., Gatesman, T. A., & Douglas, T. A. (2017). Glacierized headwater streams as aquifer recharge corridors, subarctic Alaska. *Geophysical Research Letters*, *44*, 6876–6885. https://doi.org/10.1002/2017GL073834

Littell, J. S., McAfee, S. A., & Hayward, G. D. (2018). Alaska snowpack response to climate change: Statewide snowfall equivalent and snowpack water scenarios. *Water*, *10*(5), 668. https://doi.org/10.3390/w10050668

Lundquist, J. D., Cayan, D. R., & Dettinger, M. D. (2004). Spring onset in the Sierra Nevada: When is snowmelt independent of elevation? *Journal of Hydrometeorology*, *5*, 327–342. https://doi.org/10.1175/1525-7541(2004)005<0327:SOITSN>2.0.CO;2

Markon, C., Gray, S., Berman, M., Eerkes-Medrano, L., Hennessy, T., Huntington, H., et al. (2018). Alaska. In D. R. Reidmiller, C. W. Avery, D. R. Easterling, K. E. Kunkel, K. L. M. Lewis, T. K. Maycock, & B. C. Stewart (Eds.), *Impacts, risks, and adaptation in the United States: Fourth national climate assessment* (*II*, pp. 1185–1241). Washington, DC: U.S. Global Change Research Program. https://doi.org/10.7930/NCA4.2018.CH26

Mastin, M. C., Konrad, C. P., Veilleux, A. G., & Tecca, A. E. (2016). Magnitude, frequency, and trends of floods at gaged and ungaged sites in Washington, based on data through water year 2014 (ver 1.1) (Scientific Investigations Report 2016–5118). Reston, VA: U.S. Geological Survey. https://doi.org/10.3133/sir20165118

Matti, B., Dahlke, H. E., Dieppois, B., Lawler, D. M., & Lyon, S. W. (2017). Flood seasonality across Scandinavia—Evidence of a shifting hydrograph? *Hydrological Processes*, *31*, 4354–4370. https://doi.org/10.1002/hyp.11365

McAfee, S., Guentchev, G., & Eischeid, J. (2014). Reconciling precipitation trends in Alaska: 2. Gridded data analyses. *Journal of Geophysical Research: Atmospheres*, *119*, 13820–13837. https://doi.org/10.1002/2014JD022461

McAfee, S. A., Guentchev, G., & Eischeid, J. K. (2013). Reconciling precipitation trends in Alaska: 1. Station based analyses. *Journal of Geophysical Research: Atmospheres*, *118*, 7523–7541. https://doi.org/10.1002/jgrd.50572

McCabe, G. J., Clark, M. P., & Hay, L. E. (2007). Rain-on-snow events in the western United States. *Bulletin of the American Meteorological Society*, *88*(3), 319–328. https://doi.org/10.1175/BAMS-88-3-319

Milner, A. M., Brown, L. E., & Hannah, D. M. (2009). Hydroecological response of river systems to shrinking glaciers. *Hydrological Processes*, *23*, 62–77. https://doi.org/10.1002/hyp.7197

Mundhenk, B. D., Barnes, E. A., Maloney, E. D., & Nardi, K. M. (2016). Modulation of atmospheric rivers near Alaska and the U.S. West Coast by northeast Pacific height anomalies. *Journal of Geophysical Research: Atmospheres*, *121*, 12751–12765. https://doi.org/10.1002/2016JD025350

National Aeronautics and Space Administration Land Processes Distributed Archive Center. (2011). *ASTER global digital elevation model version 2: U.S.*. Sioux Falls, SD: Geological Survey/Earth Resources Observation and Science (EROS) Center.

National Oceanic and Atmospheric Administration. (2019). *NCEI map application—Version 2.3.1. Daily observational data map*. Accessed March 29, 2019 to August 8, 2019. https://gis.ncdc.noaa.gov/maps/ncei/cdo/daily

Olden, J. D., Kennard, M. J., & Pusey, B. J. (2012). A framework for hydrologic classification with a review of methodologies and applications in ecoyhydrology. *Ecohydrology*, *5*, 503–518. https://doi.org/10.1002/eco.251

Pan, C. G., Kirchner, P. B., Kimball, J. S., Kim, Y., & Du, J. (2018). Rain-on-snow events in Alaska, their frequency and distribution from satellite observations. *Environmental Research Letters*, *13*(7), 075004. https://doi.org/10.1088/1748-9326/aac9d3

Papineau, J., & Holloway, E. (2011). *The nature of heavy rain and flood events in Alaska* (Anchorage Forecast Office Research Papers). Anchorage, AK: NOAA, National Weather Service Alaska Regional Headquarters. http://citeseerx.ist.psu.edu/viewdoc/download?doi=10.1.1.729.6444&rep=rep1&type=pdf

Pardé, M. (1933). *Fleuves et Rivières*. Paris: Armand Colin.

Poff, N. L., Allan, J. D., Bain, M. B., Karr, J. R., Prestegaard, K. L., Richter, B. D., et al. (1997). The natural flow regime: A paradigm for river conservation and restoration. *BioScience*, *47*(11), 769–784. https://doi.org/10.2307/1313099

PRISM Climate Group. (2002). *Western Canada average monthly or annual precipitation, 1961–1990 (gridded climate data)*. Corvallis, OR: Oregon State University. http://prism.oregonstate.edu/projects/canw.php

R Core Team. (2018). *R: A language and environment for statistical computing*. Vienna, Austria: R Foundation for Statistical Computing. https://www.R-project.org/

RGI Consortium. (2012). *Randolph glacier inventory—A dataset of global glacier outlines: Version 2.0* (GLIMS Technical Report). CO, USA: Global Land Ice Measurements from Space. https://doi.org/10.7265/N5-RGI-60

RGI Consortium. (2017). *Randolph glacier inventory—A dataset of global glacier outlines: Version 6.0* (GLIMS Technical Report). Colorado, USA: Global Land Ice Measurements from Space. https://doi.org/10.7265/N5-RGI-60

Rousseeuw, P. J. (1987). Silhouettes: A graphical aid to the interpretation and validation of cluster analysis. *Journal of Computational and Applied Mathematics*, *20*, 53–65. https://doi.org/10.1016/0377-0427(87)90125-7

Ryberg, K. R., Akyüz, F. A., Wiche, G. J., & Lin, W. (2016). Changes in seasonality and timing of peak streamflow in snow and semi-arid climates of the north-central United States, 1910–2012. *Hydrological Processes*, *30*, 1208–1218. https://doi.org/10.1002/hyp.10693

Sergeant, C. J., Falke, J. A., Bellmore, R. A., Bellmore, J. R., & Crumley, R. L. (2020). A classification of streamflow patterns across the coastal Gulf of Alaska. *Water Resources Research*, *56*, e2019WR026127. https://doi.org/10.1029/2019WR026127

Shanley, C. S., & Albert, D. M. (2014). Climate change sensitivity index for Pacific Salmon Habitat in Southeast Alaska. *PLoS One*, *9*(8), e104799. https://doi.org/10.1371/journal.pone.0104799

Sharma, A. R., & Déry, S. J. (2019). Variability and trends of landfalling atmospheric rivers along the Pacific Coast of northwestern North America. *International Journal of Climatology*, *40*, 544–558. https://doi.org/10.1002/joc.6227

Shulski, M., & Wendler, G. (2007). *The climate of Alaska*. Fairbanks, AK: University of Alaska Press.

Slater, L. J., & Villarini, G. (2016). Recent trends in U.S. flood risk. *Geophysical Research Letters*, *43*, 12428–12436. https://doi.org/10.1002/2016GL071199

Stewart, B., Kunkel, K., Champion, S., Frankson, R., Stevens, L., & Wendler, G. (2017). *Alaska State Climate Summary* (Tech. Rep. NESDIS 149-AK). NOAA National Oceanic and Atmospheric Administration. https://statesummaries.ncics.org/chapter/ak/

Todd, M. J., Wigington, P. J., Jr., & Sproles, E. A. (2017). Hydrologic landscape classification to estimate Bristol Bay, Alaska watershed hydrology. *Journal of the American Water Resources Association*, *53*(5), 1008–1031. https://doi.org/10.1111/1752-1688.12544

U.S. Geological Survey. (2019). *USGS water data for the nation: National Water Information System database*, U.S. Geological Survey. Accessed November 26, 2019. https://doi.org/10.5066/F7P55KJN

Valentin, M. M., Hogue, T. S., & Hay, L. E. (2018). Hydrologic regime changes in a high-latitude glacierized watershed under future climate conditions. *Water*, *10*(2), 128. https://doi.org/10.3390/w10020128

Viereck, L. A., Dyrness, C. T., Batten, A. R., & Wenzlick, K. J. (1992). *The Alaska vegetation classification* (General Tech. Rep. PNW-GTR-286). Portland, OR: U.S. Department of Agriculture, Forest Service, Pacific Northwest Research Station. https://doi.org/10.2737/PNW-GTR-286

Vormoor, K., Lawrence, D., Heistermann, M., & Bronstert, A. (2015). Climate change impacts on the seasonality and generation processes of floods—Projections and uncertainties for catchments with mixed snowmelt/rainfall regimes. *Hydrology and Earth System Sciences*, *19*, 913–931. https://doi.org/10.5194/hess-19-913-2015

Vormoor, K., Lawrence, D., Schlichting, L., Wilson, D., & Wong, W. K. (2016). Evidence for changes in the magnitude and frequency of observed rainfall vs. snowmelt driven floods in Norway. *Journal of Hydrology*, *538*, 33–48. https://doi.org/10.1016/j.jhydrol.2016.03.066

Walsh, J. E., Bhatt, U. S., Littell, J. S., Leonawicz, M., Lindgren, M., Kurkowski, T. A., et al. (2018). Downscaling of climate model output for Alaskan stakeholders. *Environmental Modelling & Software*, *110*, 38–51. https://doi.org/10.1016/j.envsoft.2018.03.021

Walsh, J. E., Overland, J. E., Groisman, P. Y., & Rudolf, B. (2011). Ongoing climate change in the Arctic. *Ambio*, *40*(Suppl. 1), 6–16. https://doi.org/10.1007/s13280-011-0211-z

Weingartner, R., Blöschl, G., Hannah, D. M., Marks, D. G., Parajka, J., Pearson, C. S., et al. (2013). Prediction of seasonal runoff in ungauged basins. In G. Blöschl, M. Sivapalan, T. Wagener, A. Viglione, & H. Savenije (Eds.), *Runoff prediction in ungauged basins: Synthesis across processes, places and scales* (pp. 102–134). Cambridge: Cambridge University Press. https://doi.org/10.1017/CBO9781139235761.009

Wilby, R. L., & Keenan, R. (2012). Adapting to flood risk under climate change. *Progress in Physical Geography: Earth and Environment*, *36*(3), 348–378. https://doi.org/10.1177/0309133312438908

Wiley, J. B., & Curran, J. H. (2003). *Estimating annual high-flow statistics and monthly and seasonal low-flow statistics for ungaged sites on streams in Alaska and conterminous basins in Canada* (Water-Resources Investigations Report 03-4114). Anchorage, AK: U.S. Geological Survey. https://doi.org/10.3133/wri034114

Wouters, G., Gardner, A. S., & Moholdt, G. (2019). Global glacier mass loss during the GRACE satellite mission (2002–2016). *Frontiers of Earth Science*, *7*, 96. https://doi.org/10.3389/feart.2019.00096